Journal of Molecular Structure 993 (2011) 57–61

Contents lists available at ScienceDirect

Journal of Molecular Structure

journal homepage: www.elsevier.com/locate/molstruc

Discrimination between basal cell carcinoma and hair follicles in skin tissue sections by Raman micro-spectroscopy

M. Larraona-Puy [a], A. Ghita [a], A. Zoladek [a], W. Perkins [b], S. Varma [b], I.H. Leach [c], A.A. Koloydenko [d], H. Williams [e], I. Notingher [a,*]

[a] School of Physics and Astronomy, University of Nottingham, University Park, NG7 2RD Nottingham, UK
[b] Dermatology Department, Nottingham University Hospital NHS Trust, QMC Campus, Derby Road, NG7 2UH Nottingham, UK
[c] Histopathology Department, Nottingham University Hospital NHS Trust, QMC Campus, Derby Road, NG7 2UH Nottingham, UK
[d] Mathematics Department, Royal Holloway, University of London, Egham TW20 0EX, UK
[e] Centre of Evidence-Based Dermatology, C Floor South Block, Nottingham University, Hospital NHS Trust, QMC Campus, Derby Road, NG7 2UH Nottingham, UK

ARTICLE INFO

Article history:
Available online 3 November 2010

Keywords:
Raman micro-spectroscopy (RMS)
Basal cell carcinoma (BCC)
Mohs micrographic surgery (MMS)
Hair follicle
Automated histopathology

ABSTRACT

Skin cancer is the most common human malignancy and basal cell carcinoma (BCC) represents approximately 80% of the non-melanoma cases. Current methods of treatment require histopathological evaluation of the tissues by qualified personnel. However, this method is subjective and in some cases BCC can be confused with other structures in healthy skin, including hair follicles. In this preliminary study, we investigated the potential of Raman micro-spectroscopy (RMS) to discriminate between hair follicles and BCC in skin tissue sections excised during Mohs micrographic surgery (MMS). Imaging and diagnosis of skin sections was automatically generated using '*a priori*'-built spectral model based on LDA. This model had 90 ± 9% sensitivity and 85 ± 9% specificity for discrimination of BCC from dermis and epidermis. The model used selected Raman bands corresponding to the largest spectral differences between the Raman spectra of BCC and the normal skin regions, associated mainly with nucleic acids and collagen type I. Raman spectra corresponding to the epidermis regions of the hair follicles were found to be closer to those of healthy epidermis rather than BCC. Comparison between Raman spectral images and the gold standard haematoxylin and eosin (H&E) histopathology diagnosis showed good agreement. Some hair follicle regions were misclassified as BCC; regions corresponded mainly to the outermost layer of hair follicle (basal cells) which are expected to have higher nucleic acid concentration. This preliminary study shows the ability of RMS to distinguish between BCC and other tissue structures associated to healthy skin which can be confused with BCC due to their similar morphology.

1. Introduction

Mohs micrographic surgery (MMS) is the current gold standard treatment for large, aggressive, recurrent and ill-delimited cases of continuous basal cell carcinoma (BCC) [1,2]. MMS is a surgical technique consisting of several sequential steps where tumour borders are carefully localized by a close microscopic follow-up. In MMS, consecutive layers of tissue are excised one at a time, parallel to the skin surface. Each layer is histopathologically examined before the next layer is excised. This maximizes healthy tissue conservation without compromising total tumour removal. The process continues until all sections are clear of cancer, which on average requires from 2/3 h up to 1 day. For the cases where other more accessible techniques have a lower rate of success, MMS is considered more cost-effective due to its maximal conservation of healthy tissue and exceptional cosmetic results [2,3]. However, a main limitation of MMS is its reliability on histopathology examination of tissue sections. Histopathology is a subjective, non-automated time-consuming technique where trained specialists diagnose the presence or absence of cancer by reading the histological slides acquired from a biopsy specimen. Diagnosis relies on the experience of the trained histopathologist, which is prone to interobserver variability [4,5]. In practice, the interpretation of MMS sections is mostly performed by the surgeon, which may be subject to diagnostic errors. Interobserver differences have been widely reported since histopathology has become a routinely clinical technique [6]. Refs. [7,8] are studies on 48 and 592 samples, respectively. The former was evaluated by 20 histopathologists with an 87% overall sensitivity and 94% specificity and the latter by two histopathologists with 93% agreement. These rates will vary depending on the difficulty of the samples being studied and the efficiency of sample preparation, especially the sectioning procedure [9].

* Corresponding author. Tel.: +44 (0)11595 15172.
E-mail address: ioan.notingher@nottingham.ac.uk (I. Notingher).

0022-2860/$ - see front matter © 2010 Elsevier B.V. All rights reserved.
doi:10.1016/j.molstruc.2010.10.046

The most common sample preparation includes tissue freezing, sectioning, fixation, and staining with haematoxylin and eosin (H&E). In H&E treated samples, some skin structures such as inflammation, hair follicles or benign tumours might be confused with certain BCC subtypes due to its apparent morphological similarity and colour after staining [9,10]. Examples of H&E skin tissue specimens with straightforward and difficult diagnosis are shown in Fig. 1. In particular, Fig. 1b shows an example of skin tissue containing BCC and hair follicle, where structures resemble morphologically.

Other methods used to stain MMS fresh-frozen tissue sections are toluidine blue (TB) and methylene blue (MB) [11]. TB and MB tend to accumulate in the mitochondria of carcinoma cells to a greater extent than in normal cells. TB is technically easier and responds faster than H&E [12]. A recent preliminary study comparing H&E and TB staining methods in MMS excised tissue sections recommended the latter for BCC identification [13]. TB can be helpful in discriminating basaloid cells around hair follicles from false apparent cases of BCC [13]. It visualises stromal change, which might be an indicator of residual BCC. In particular TB stains mucin, a protein generally only present in tissue adjacent to BCC and not to the follicular structures, with the exception of the dermal papilla [9,13]. In addition, TB stains the inner root shear of hair follicles deep blue, which facilitates its visualization [13]. Despite all of these advantages, TB is only used by 16.8% of Mohs' surgeons surveyed, thus H&E is the standard staining method [14]. The main reason for this choice is that H&E is the most common staining technique used in their training [13,14].

Hair follicles are tubular invaginations of the epidermis extending deep into the dermis that surrounds the root of the hair. The terminal expanded part of the follicle is called the hair bulb. At the base of the follicle there is a projection called dermal papilla containing capillaries that irrigate the cells in the bulb. Those cells are mitotically active, overcoming differentiation and keratinisation and thus generating the hair fibre or hair shaft [15]. The hair shaft is a long filament in the centre of the follicle extended above the surface of the epidermis that is composed of three layers (medulla, cortex and cuticle). Those layers consist of keratotic protein, (65–95%), water, lipids, melanin pigment granules and trace elements [15,16]. In our study, we will use the term hair to refer to the hair shaft, and we will differentiate this structure from the hair follicle. BCCs may manifest a keratin profile similar to that of the lower part of the hair follicle and different to hair [17].

Tissue images produced by spectroscopic techniques such as fluorescence, infrared or Raman include sample chemical information. Thus, their use is especially interesting for the classification of structures that mimic BCC. Many studies based on fluorescence imaging have been reported to discriminate BCC from healthy tissue [18–21]. Nevertheless, fluorescence imaging has several intrinsic disadvantages when compared to vibrational spectroscopy, namely chemical labelling, broader spectra and lack of quantification. Fluorescence imaging provides purely qualitative information as it relies on emission intensity spectra, which highly depends on sample preparation and photobleaching.

Vibrational spectroscopy techniques such as infrared and Raman spectroscopy achieve high chemical specificity and tumour discrimination accuracy, presenting spectra with sharp meaningful peaks. An early study with IR micro-spectroscopy showed 93% sensitivity in discrimination among epidermis, BCC, squamous cell carcinoma and melanocytic lesions [22]. BCC-epidermis discrimination was based on BCC higher nucleic acid concentration. However, the main limitation of IR resides in sampling thickness, which cannot be larger than 10 μm to avoid complete absorption of the incident radiation by the tissue [23,24].

Raman micro-spectroscopy (RMS) allows both high chemical specificity and resolution on thick specimens, as the Raman signal is produced by inelastic scattering of monochromatic light by the atoms and molecules in the sample. The potential of RMS in skin cancer detection has been widely reported in the last twenty years [24–28]. Slight biochemical changes appearing in cells presenting dysplasia, such as increased nucleus-to cytoplasm ratio, disordered chromatin, higher metabolic activity and alterations in lipid and protein levels are detected with RMS [29].

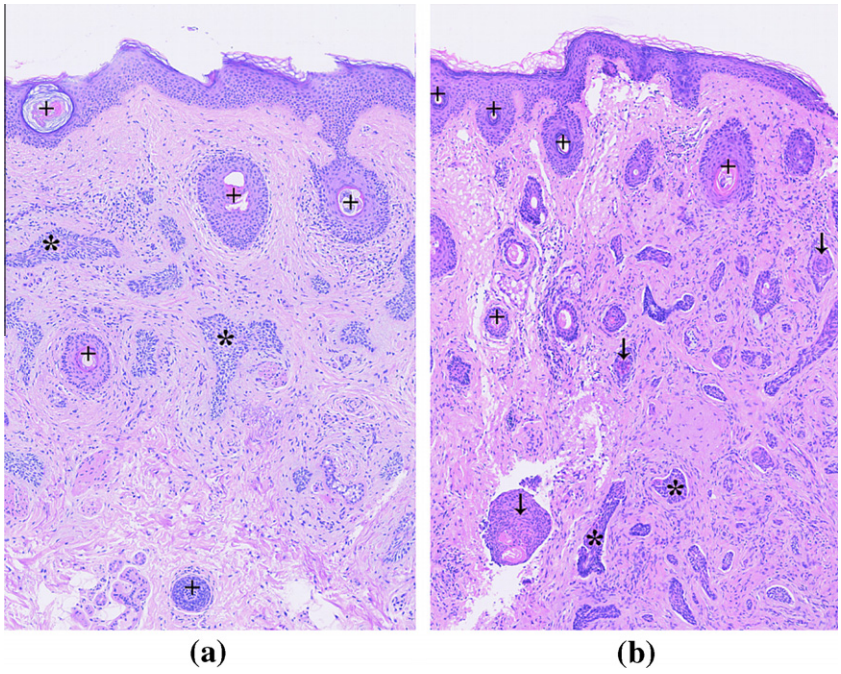

Fig. 1. H&E images of two MMS sections of skin tissue were hair follicle–BCC diagnosis is (a) straightforward to the trained histopathologist, and (b) difficult to discriminate. Symbol code: crosses (+) over easy-to-diagnose hair follicles, asterisks (*) over clear BCC regions and arrows (↓) pointing regions where diagnosis is difficult and not clear.

In a previous study, we showed how RMS assisted by supervised classification models can be used for detection and imaging of BCC in skin tissue sections excised during MMS. The model was utilized to build quantitative 2-D biochemical images of unknown skin tissue samples. The automatic pseudocolour images revealed the presence/absence of a tumour without the need for a histopathologist and accurately pinpointed its location [28].

In this preliminary study, we investigated the potential of Raman micro-spectroscopy to discriminate between hair follicle and basal cell carcinoma in excised skin tissue sections during Mohs micrographic surgery. Imaging and automated diagnosis of skin sections was automatically generated by using '*a priori*'-built spectral model based on LDA [28]. RMS has revealed the spectral differences between hair follicle, hair, sweat ducts, capillaries, sebaceous glands, dermis and BCC [16,30], but no supervised classification models able to produce quantitative spectra images and automatic diagnosis were developed.

2. Experimental

2.1. Skin samples

Skin tissue sections were obtained from the Nottingham University Hospitals National Health Service (NHS) Trust. Consent was obtained from the patients and ethical approval was granted from Nottingham Research Ethics Committee. Tissue sections were cut from blocks removed during MMS and standard BCC excision into 20 μm sections for RMS investigations. After the RMS measurements, the analysed sections were stained using haematoxylin and eosin (H&E). Diagnosis was carried out by a consultant dermatopathologist.

2.2. Instrumental set-up

The customized Raman microspectrometer was built as described in our previous work (see [28]). Sample illumination was performed by a 785-nm continuous wave GaAs diode laser (XTRA, Toptica Photonics, Munich, Germany), coupled to an inverted microscope (IX71, Olympus, Essex, United Kingdom) with a 50× objective lens (N.A. 0.75) and an automated translation stage (H117, Prior Ltd., Cambridge, United Kingdom). Additionally, the system incorporates a spectrograph (SR-303i, Andor Ltd., Belfast, United Kingdom) and a deep-depletion back-illuminated charged coupled device (DU401A-BR-DD, Andor Ltd., Belfast, United Kingdom).

2.3. Data acquisition

Areas of fresh tissue sections (approximately 500 μm by 500 μm) containing BCC, epidermis, dermis and hair follicles were raster scanned (5 μm step size) with 2 s acquisition time at each position. After the measurement, the sections were H&E stained and diagnosed by a consultant histopathologist using the same microscope employed for acquisition of the Raman spectral images. The accuracy of the sample retroposition on the microscope was 5 μm, as measured using two engraved marks on the slides.

2.4. Analysis

All spectra were analysed using functions developed in MATLAB software (version 7.6.0.324, MathWorks). The pre-processing consisted of a sixth-order polynomial baseline correction, normalized to zero mean and unity standard deviation and smoothed using the Savitsky–Golay algorithm (five points, second-order polynomial). Cosmic rays were removed by semi-automatic customized MATLAB programs. Raman spectra of the MgF_2 substrate were detected using a threshold filter in the 1370–1500 cm^{-1} spectral range and eliminated from the classification model.

Data analysis was performed using the multi-step classification model reported on Ref. [28]. Firstly, spectral data reduction was performed by selecting the Raman spectral bands which provide maximum differences among the classes under study. In second place, the reduced data set was input into a two-step classifier. Two consecutive linear discriminant analysis (LDA) were performed to discriminate between dermis and the other classes and then, between BCC and epidermis.

RMS analysis on the selected fresh-tissue samples was performed with our own MATLAB package. Each spectrum was preprocessed in analogy to the model database. Spectra were binned to account for tissue heterogeneity, achieving a spatial resolution of 10 μm. The region of the image containing hair was guided by the diagnosed H&E image, and their spectra separated for an independent analysis. The LDA model was then applied to predict the class of each spectrum as BCC, epidermis, or dermis, building the image. Spectra from the images representing the three classes detected by the model were normalized to the model database for posterior comparison.

3. Results and discussion

3.1. Classification model

In a previous report [28], it was found that maximum spectral differences between BCC, epidermis and dermis were achieved by using the ratios of the following Raman bands:

$$r_1 = \frac{I_{788\ cm^{-1}}}{I_{1003\ cm^{-1}}}, \quad r_2 = \frac{I_{850\ cm^{-1}}}{I_{1003\ cm^{-1}}}, \quad r_3 = \frac{I_{950\ cm^{-1}}}{I_{1003\ cm^{-1}}}, \quad r_4 = \frac{I_{1093\ cm^{-1}}}{I_{1003\ cm^{-1}}}, \quad r_5 = \frac{I_{1312\ cm^{-1}}}{I_{1268\ cm^{-1}}}. \tag{1}$$

These Raman bands were assigned to molecular vibrations of collagen type I (amide III spectral regions from 1200 to 1350 cm^{-1}) and DNA (the 788 and 1093 cm^{-1} bands corresponding to the O–P–O phosphodiester and PO_2 vibrations in DNA, respectively) [31]. In addition, Raman bands at 850 and 950 cm^{-1} were associated to proline and C–C backbone vibrations in proteins [32]. Intensity of the 1003 cm^{-1} band corresponding to the ring breathing of phenylalanine was chosen as denominator of the ratios due to its invariability among all measurements.

The model showed that RMS is able to discriminate nodular and morphoeic BCC from healthy tissue with 90 ± 9% sensitivity and 85 ± 9% specificity in split cross-validation algorithms.

3.2. Raman spectral imaging

Fig. 2 shows the H&E image of a typical skin section excised during MMS which contained BCC, epidermis, dermis and hair. The left image of Fig. 2 is an H&E image of the MMS-excised sample, with the labels included after histopathological diagnosis. Standard H&E technique uses haematoxylin to stain cell nuclei in purple or black, depending on the type of haematoxylin and on section thickness, and eosin to counterstain the sample, turning cytoplasmatic proteins into pink or red[1] [33]. In skin samples, a range of tones from black to red will appear depending on sample composition: dermal collagen turns into pale pink, muscle into deep pink, cytoplasm pink to red, and cancer cells, epidermis and inflammation, blue.

[1] For interpretation of colour in Fig. 2, the reader is referred to the web version of this article.

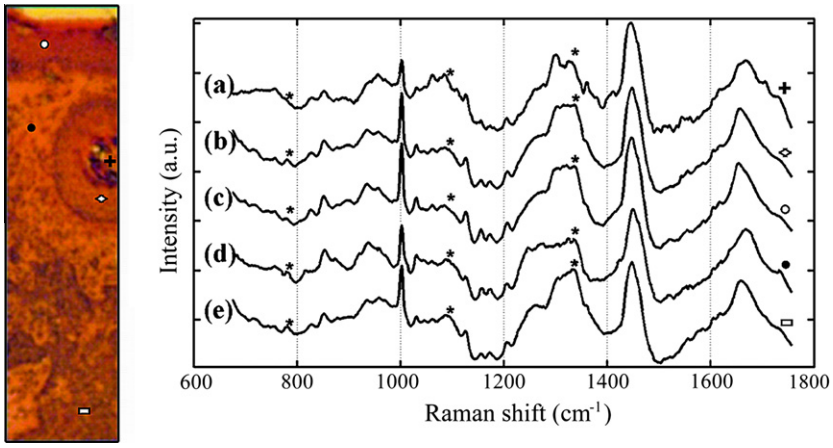

Fig. 2. Right: Raman spectra of different regions within a skin tissue section. The labels correspond: (a) to hair, (b) to hair follicle, (c) to epidermis, (d) to dermis and (e) to BCC. Asterisks correspond to main DNA peaks and collagen peak. Left: H&E image of the skin tissue section from where the Raman spectra where taken. Symbol code: empty circle for epidermis (○); filled circle for dermis (●); empty rhombus for hair follicle (◇); rectangle for BCC (□) and cross for hair (+).

Hair follicles will adopt the same blue colour as the external epidermis layer as they are mainly composed by epidermis.

However, the images included in this study showed DNA in dark brown and dermis in pale orange as an effect of the CCD camera calibration. Regions with higher DNA will be darker, as it is the case of cancerous areas. On the contrary, regions with higher collagen will present a paler colour, as it is the case of dermis. Regions with inflammation, epidermis and hair follicles will adopt similar colour than BCC. Therefore, in samples with BCC, epidermis surrounding hair follicles might be confused with malignant tissue due to its morphological resemblance, especially if the H&E stained slides are a tangential cut of the hair follicle, showing its base. In these specific cases, epidermis forming the hair follicle that appears in the hair cross-section tend to present a solid circular BCC-like shape, and not a specific hollow ring easily-diagnosed form .

Mean Raman spectra measured at regions corresponding to each feature are presented and asterisks have been introduced to highlight the Raman bands at 788 cm^{-1}, 1093 cm^{-1} and 1350 cm^{-1}, which have previously been assigned to the main peaks in DNA and collagen type I (see Section 3.1).

In agreement with our previous study, Fig. 2 confirms that BCC has a higher amount of DNA compared to the other tissue regions, which was associated to the higher cell density in cancerous regions. The Raman spectrum of dermis is similar to the spectrum of collagen type I and shows lower contribution from DNA than epidermis and BCC (there are fewer cells in dermis).

The Raman spectra of hair and hair follicle agree with results previously reported [19]. In addition, a study by Barry et al. [34] reported the Raman bands of stratum corneum, the outermost epidermal layer, composed mainly by keratin and therefore very similar to hair Raman spectrum.

Hair had strong bands at 1447 cm^{-1}, assigned to the CH_2 deformation (protein vibration); a medium-strong band around 1667 cm^{-1}, assigned to the in-plane peptide carbonyl stretching vibration (C═O stretch) in the amide I band; a medium band at 1003 cm^{-1}, associated to the aromatic ring C–C stretching mode of phenylalanine; a strong-medium peak at 1300 cm^{-1} assigned to the deformation mode of the CH_2 and two medium broad peaks at 1324 and 1330 cm^{-1} that might be due to the CH_3CH_2 wagging mode in purine bases of DNA and to phospholipids or DNA [35]. Smaller peaks were measured at 829 cm^{-1}, 852 cm^{-1}, 956 cm^{-1}, 1032 cm^{-1}, 1061 cm^{-1}, 1085 cm^{-1}, 1126 cm^{-1}, 1155 cm^{-1}, 1173 cm^{-1} and 1206 cm^{-1}, which may be due to, aliphatic and aromatic deformation of CCH, CH_2 rock, CH_3 rock or olefinic deformation of CCH, skeletal vibrations of CC, COH deformation, again CC vibrations and CH_2 deformation, respectively. A weak broad peak was found at 890 cm^{-1}, probably associated to CH_2 rock. Finally a shoulder was detected at 1360 cm^{-1}, which might be due to tryptophan. Results are consistent with the previous studies [16,34].

The Raman spectrum of hair follicle (Fig. 2b) is very similar to the measured spectrum of the epidermal layer (Fig. 2c) and is consistent with the anatomical description included in the introduction (see Section 1).

To identify the differences between epidermis, BCC and hair follicles, the computed difference spectra between BCC and hair follicles and BCC and epidermis are presented in Fig. 3 and compared to the Raman spectrum of purified DNA. Asterisks highlight the main DNA peaks which can also be observed in the difference spectrum. It can be observed that the Raman spectrum of hair follicle has a higher similarity to epidermis than to BCC as BCC has a higher contribution from DNA peaks, from where it can be inferred that a higher amount of DNA is present in the tumour tissue. As we reported before, this is caused by the smaller amount of cytoplasm and higher density of cells present in the tumour [28], and agrees with the H&E image shown in Fig. 2.

These spectral differences between hair follicles and BCC were used to produce spectral images of skin tissues, with the aim to discriminate BCC from hair follicles.

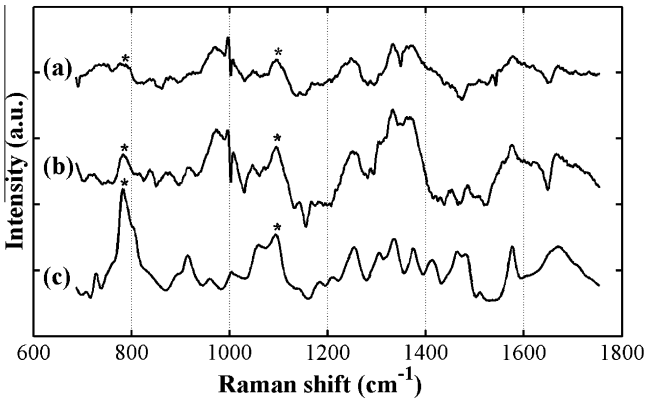

Fig. 3. Raman spectra of (a) difference between BCC and hair follicle spectra, (b) difference between BCC and epidermis spectra and (c) DNA. Asterisks correspond to main DNA peaks.

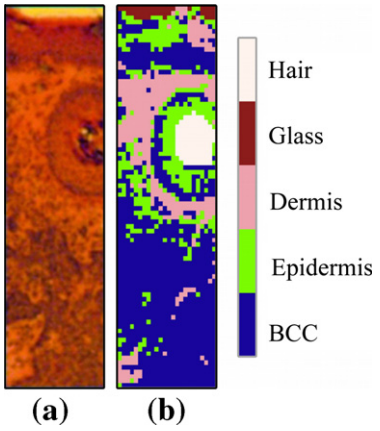

Fig. 4. (a) H&E image of the skin tissue section from Fig 2; (b) Raman spectral image obtained by using the LDA classification model.

Raman spectral images of skin samples with hair and hair follicle were produced using the classification model described previously. Fig. 4 shows the comparison between the Raman spectral image and the H&E image of the same tissue section. The spatial resolution of the Raman spectral image is 10 μm. Fig. 4 shows a good agreement between the Raman spectral imaging and the gold standard, showing good classification of BCC, epidermis, dermis and hair follicles. In particular, the majority of hair follicle and epidermis was classified as epidermis. This result agrees with the fact that hair follicle is an invagination of normal epidermis. The presence of BCC is also correctly predicted, however some misclassifications as false positives were found, in particular for regions of epidermis and hair follicles with higher DNA concentration, as observed in the H&E image. These regions were mainly found at the edges of the epidermis. This might be explained by the high sensitivity in cancer detection, which needs to include all the outline cases, consequently lowering the specificity of our model. Dermis is also correctly predicted, cases presenting inflammation being several times misclassified as epidermis, due to the high concentration of cells.

However, misclassification errors can be eliminated by using anatomical information of healthy skin and BCC. Misclassification of epidermis with BCC was in the edges of the hair bulb, which corresponds to the basal cells of the epithelium. These cells have less cytoplasm and an increased nucleus-to-cytoplasm ratio than the rest of the cells in the hair follicle. Consequently a higher DNA concentration might be expected in this region, as predicted by our model. Furthermore, as BCC arises from the basal layer, it is likely to resemble to basal cells and *vice versa*, not only morphologically but also from a chemical point of view.

4. Conclusions

This paper shows a preliminary study of RMS using supervised classification models for discriminating BCC from hair follicles in skin tissue sections excised during MMS. We have developed an optical method able to automatically diagnose particular skin structures that present a clinical challenge to trained histopathologists. The introduction of RMS as an optical diagnostic tool to enhance chemical information from a MMS sample is especially interesting in these cases were morphological information is not sufficient to discriminate between normal skin structures and a malignant lesion.

A previously developed LDA-model based on supervised Raman band selection (BCC discrimination with 90 ± 9% sensitivity and 85 ± 9% specificity) was used in this study to create automated Raman spectral images and provide diagnosis for new skin tissue sections containing BCC, dermis, epidermis and hair follicles. The Raman spectrum of hair follicles had a higher amount of nucleic acids than the external epithelial layer spectrum. Raman spectral images showed excellent agreement with H&E diagnosed images. However, further studies are required to measure Raman spectra from a large number of hair follicle samples, as well as other structures found in healthy skin but often misdiagnosed as BCC, and include these structures as separate classes in the classification models. Such models are more likely to provide a higher diagnosis accuracy for BCC.

Acknowledgments

The authors would like to acknowledge the financial support of the UK National Institute for Health Research (NEAT FSG004), the University of Nottingham Hospitals Charity and the Engineering Physical Sciences Research Council (Bridging the Gaps Grant EP/E018580/1).

References

[1] F.E. Mohs, Arch. Surg. 42 (1941) 279–295.
[2] K. Nouri, A. Patel, V. Vejjabhinanta, in: K. Nouri (Ed.), Skin Cancer, Mc Graw-Hill, 2008, p. 482.
[3] T.L. Bialy, J. Whalen, E. Veledar, D. Lafreniere, J. Spiro, T. Chartier, S.C. Chen, Arch. Dermatol. 140 (2004) 736–742.
[4] A.B. Fleischer, S.R. Feldman, J.O. Barlow, B. Zheng, H.B. Hahn, T.Y. Chuang, K.S. Draft, L.E. Golitz, E. Wu, A.S. Katz, J.C. Maize, T. Knapp, J. Am. Acad. Dermatol. 44 (2) (2001) 224–230.
[5] A. Hernández-Martín, D. Arias-Palomo, E. Barahona, C. Hidalgo, C. Muñoz, Actas Dermo-Sifiliográficas 98 (10) (2007) 694–701.
[6] M. Mogensen, G.B.E. Jemec, Dermatol. Surg. 33 (2007) 1158–1174.
[7] L. Brochez, E. Verhaeghe, E. Grosshans, E. Haneke, G. Piérard, D. Ruiter, J.-M. Naeyaert, J. Pathol. 196 (2002) 459–466.
[8] M.J. Trotter, A.K. Bruecks, Arch. Pathol. Lab. Med. 127 (2003) 1489–1492.
[9] H.A. Horiba, M.B. Morgan, in: S.N. Snow, G.R. Mikhail (Eds.), Mohs Micrographic Surgery, W.B. Saunders, Philadelphia, 1991, p. 341.
[10] E. Stockfleth, C. Surbert, C. Ulrich, Br. J. Dermatol. 161 (s3) (2009) 1–5.
[11] A.N. Yaroslavsky, V. Neel, R.R. Anderson, J. Invest. Dermatol. 121 (2003) 259–266.
[12] O. Arnon, A.J. Mamelak, L.H. Goldberg, in: K. Gross, H.K. Steinman (Eds.), Mohs Surgery and Histopathology: Beyond the Fundamentals, Cambridge University Press, New York, 2009, pp. 155–160.
[13] T.R. Humphreys, A. Nemeth, S. McCrevey, S.C. Baer, L.H. Goldberg, Dermatol. Surg. 22 (2008) 693–697.
[14] M.M. Todd, J.W. Lee, Dermatol. Surg. 31 (2) (2006) 244–245.
[15] Gunasegaran (Ed.), Textbook of Histology and a Practical Guide, Elsevier, New Delhi, 2007, p. 165.
[16] W. Akhtar, H.G.M. Edwards, D.W. Farwell, M. Nutbrown, Spectrochim. Acta Part A 53 (1997) 1021–1031.
[17] N. Crowson, Mod. Pathol. 19 (2006) S127–S147.
[18] L. Brancaleon, A.J. Durkin, J.H. Tu, G. Menaker, J.D. Fallon, N. Kollias, Photochem. Photobiol. 73 (2001) 178–183.
[19] M. Al-Arashi, E. Salomatina, A.N. Yaroslavsky, Lasers Surg. Med. 39 (2007) 696–705.
[20] D. Gareau, J. Biomed. Opt. 13 (5) (2008) 054001.
[21] B. Stenquist, M.B. Ericson, L. Molne, A. Rosen, O. Larko, A.M. Wennberg, Br. J. Dermatol. 154 (2006) 305–309.
[22] L.M. McIntosh, M. Jackson, H.H. Mantsch, M.F. Stranc, D. Pilavdzic, A.N. Crowson, J. Invest. Dermatol. 112 (1999) 951–956.
[23] L.M. McIntosh, R. Summers, M. Jackson, H.H. Mantsch, J. Invest. Dermatol. 116 (2001) 175–181.
[24] M. Gniadecka, H.C. Wulf, O.F. Nielsen, D.H. Christensen, J. Hercogova, Photochem. Photobiol. 66 (1997) 418–423.
[25] A. Nijssen, T.C.B. Schut, F. Heule, P.J. Caspers, D.P. Hayes, M.H. Neumann, G.J. Puppels, J. Invest. Dermatol. 119 (2002) 64–69.
[26] M. Gniadecka, J. Invest. Dermatol. 122 (2004) 443–449.
[27] C.A. Lieber, S.K. Majumder, D. Billheimer, D.l.L. Ellis, A. Mahadevan-Jansen, J. Biomed. Opt. 13 (2) (2008) 024013.
[28] M. Larraona-Puy, A. Ghita, A. Zoladek,W. Perkins, S. Varma, I. Leach, H. Williams, A.A. Koloydenko, I. Notingher, J. Biomed. Opt. 14(5) (2009) 0540311-10.
[29] M. Keller, Spectroscopy 21 (11) (2006) 33–41.
[30] P.J. Caspers, Biophys. J. 85 (1) (2003) 572–580.
[31] A.T. Tu (Ed.), Raman Spectroscopy in Biology: Principles and Applications, John Wiley and Sons, New York, 1982.
[32] B.G. Frushour, J.L. Koenig, Biopolymers 14 (2) (1975) 379–391.
[33] A. Stevens, J.S. Lowe (Eds.), Human Histology, Mosby, London, 1997.
[34] B.W. Barry, H.G.M. Edwards, A.C. Williams, J. Raman Spectrosc. 23 (1992) 641–645.
[35] Z. Movasaghi, S. Rehman, I.U. Rehman, Appl. Spectrosc. Rev. 42 (2007) 493–541.